

GROWTH RATES OF THE ELECTROSTATIC WAVES IN RADIO ZEBRA MODELS

JAN BENÁČEK¹ AND MARIAN KARLICKÝ²

¹*Department of Theoretical Physics and Astrophysics, Masaryk University, Kotlářská 2, CZ-61137 Brno, Czech Republic*

²*Astronomical Institute of the Academy of Sciences of the Czech Republic, CZ-25165 Ondřejov, Czech Republic*

ABSTRACT

Zebras were observed not only in the solar radio emission but also in radio emissions of Jupiter and Crab Nebula pulsar. In their models, growth rates of the electrostatic waves play an important role. Considering the plasma composed from the thermal background plasma and hot and rare component with the Dory-Guest-Harris distribution, we compute the growth rates γ and dispersion branches of the electrostatic waves in the $\omega - k_{\perp}$ domain. We show complexity of the electrostatic wave branches in the upper-hybrid band. In order to compare the results, which we obtained using the kinetic theory and Particle-in-cell (PIC) simulations, we define and compute the integrated growth rate Γ , where the "characteristic width" of dispersion branches was considered. We found a very good agreement between the integrated growth rates and those from PIC simulations. For maximal and minimal Γ we showed locations of dispersion branches in the $\omega - k_{\perp}$ domain. We found that Γ has a maximum when the dispersion branches not only cross the region with high growth rates γ , but when the dispersion branches in this region are sufficiently long and wide. We also mentioned the effects of changes in the background plasma and hot component temperatures.

Keywords: Instabilities – Methods: analytical – Methods: numerical
– Sun: radio radiation – planets and satellites: individual:
Jupiter – pulsars: individual (Crab Nebula pulsar)

1. INTRODUCTION

Solar radio zebras belong to the most important fine structures used in diagnostics of solar flare plasmas (Chernov 2011; Chen et al. 2011; Zlotnik 2013). Similarly, the zebras observed in the radio emission of Jupiter and Crab Nebula pulsar (Hankins & Eilek 2007; Hankins et al. 2016; Panchenko et al. 2018) can also be used for diagnostics purposes. Among many models of all these zebras, the model based on the double plasma resonance (DPR) instability belongs to the most probable (Zheleznyakov & Zlotnik 1975b; Melrose & Dulk 1982; Zaitsev & Stepanov 1983; Winglee & Dulk 1986; Ledenev et al. 2001; Zlotnik 2013; Karlický & Yasnov 2015; Zlotnik et al. 2016; Karlický & Yasnov 2018b,a).

In this model the DPR instability generates the upper-hybrid waves with the frequency

$$\omega^2 = \omega_{\text{pe}}^2 + \omega_{\text{ce}}^2 + 3k_{\perp}^2 v_{\text{tb}}^2, \quad (1)$$

when the resonance condition

$$\omega - \frac{k_{\parallel} u_{\parallel}}{\gamma_{\text{rel}}} - \frac{s\omega_{\text{ce}}}{\gamma_{\text{rel}}} = 0, \quad (2)$$

is fulfilled. Here ω , ω_{pe} , and ω_{ce} are the wave, electron-plasma, and electron-cyclotron frequency, $\mathbf{k} = (k_{\parallel}, k_{\perp})$ is wave vector, v_{tb} the thermal electron velocity of the background plasma, $\mathbf{u} = (u_{\perp}, u_{\parallel})$, $u_{\perp} = p_{\perp}/m_e$, and $u_{\parallel} = p_{\parallel}/m_e$ are the hot electron velocities perpendicular and parallel to the magnetic field; m_e is the electron mass, γ_{rel} is the relativistic Lorentz factor, s is the gyro-harmonic number, and c is the speed of light. For details, see e.g. Benáček & Karlický (2018).

In theoretical models of the double plasma resonance instability, a two-component plasma with the background plasma having the Maxwellian distribution and hot and rare component with the Dory-Guest-Harris electron distribution for $j = 1$ (Dory et al. 1965)

$$f_{\text{hot}}(u_{\parallel}, u_{\perp}) = \frac{u_{\perp}^2}{2(2\pi)^{3/2} v_{\text{t}}^5} \exp\left(-\frac{u_{\perp}^2 + u_{\parallel}^2}{2v_{\text{t}}^2}\right), \quad (3)$$

is assumed. Here v_{t} we call the thermal velocity of hot electrons, although the distribution function in this relation is not Maxwellian.

In interpretations of zebra observations, which use this model, it is usually supposed that the electron-plasma frequency is related to the electron-cyclotron frequency as follows

$$\omega_{\text{pe}} \approx s\omega_{\text{ce}}. \quad (4)$$

However, Benáček et al. (2017) showed that there can be the frequency shift from this simple equation up to 16 % for Dory-Guest-Harris velocity distribution and even higher for other velocity distributions (Yasnov et al. 2017).

Besides the zebra model based on DPR instability, there is the model that explains zebras by a nonlinear interaction of Bernstein modes (Kuznetsov 2005;

Zlotnik & Sher 2009). This model was supported by zebra observations made by Altyntsev et al. (2005). In principle, Bernstein modes can also be generated in the upper-hybrid band. Both the upper-hybrid waves and Bernstein mode are the electrostatic (longitudinal) waves. Because in the upper-hybrid band in some cases it is difficult to distinguish these waves, therefore in the following we use the general term - the electrostatic waves.

As will be shown in the following, in the upper-hybrid band (i.e., at frequencies close to the upper-hybrid frequency) there can be several dispersion branches of the unstable electrostatic waves which energy can grow simultaneously. Therefore, we define the "characteristic width" of dispersion branches and compute the wave growth rates integrated over the upper-hybrid band. Thus, for the first time we compare the results obtained using the analytical kinetic theory with the results of PIC simulations. We study the integrated growth rate in dependence on the ratio of the electron-plasma and electron-cyclotron frequency and in relation to positions of the wave dispersion branches in the $\omega - k_{\perp}$ domain. We use 3-dimensional PIC model. Note that PIC models naturally give the integrated growth rates.

The paper is structured as follows. In Section 2 we start with a theory of the electrostatic (longitudinal) waves perpendicular to the magnetic field. The integrated growth rates of these waves in the upper-hybrid band computed from the analytical relations are in Section 3. In Section 4 there are the growth rates obtained numerically. Discussion of the results and conclusions are in Sections 5.

2. ELECTROSTATIC WAVES IN THE UPPER-HYBRID BAND AND THEIR GROWTH RATES

Let us consider the plasma composed from the background Maxwellian plasma with the density n_e and the thermal velocity v_{tb} and hot plasma having the density n_h and the "thermal" velocity v_t , where $n_h \ll n_e$. Then the dispersion relation of the electrostatic (longitudinal) waves in such a plasma is given by the permittivity tensor

$$\epsilon_{\parallel} = \epsilon_{\parallel}^{(0)} + \epsilon_{\parallel}^{(1)} = 0, \quad (5)$$

where the term $\epsilon_{\parallel}^{(0)}$ corresponds to the background Maxwellian plasma and the term $\epsilon_{\parallel}^{(1)}$ is a correction to the hot and rare plasma component.

In our case with $n_h \ll n_e$ and in agreement with Chen (1974); Zheleznyakov (1997); Fitzpatrick (2015) we can write

$$\epsilon_{\parallel}^{(0)} = 1 - 2\omega_{pe}^2 \frac{e^{-\lambda}}{\lambda} \sum_{l=1}^{\infty} \frac{l^2 I_l(\lambda)}{\omega^2 - l^2 \omega_{ce}^2} = 0, \quad (6)$$

$$\omega_{pe}^2 = \frac{n_e e^2}{m_e \epsilon_0}, \quad \lambda = \frac{k_{\perp}^2 v_{tb}^2}{\omega_{ce}^2}, \quad (7)$$

where ω_{pe} and ω_{ce} is the plasma frequency of the background plasma and the electron cyclotron frequency, ϵ_0 is the permittivity of free space, λ is the dimensionless param-

eter, $I_l(\lambda)$ is the modified Bessel function of l th order, m_e is the electron mass, e is the electron charge, ω is the wave frequency, $\mathbf{k} = (k_{\parallel}, k_{\perp})$ is the wave vector parallel and perpendicular to the direction of the magnetic field, respectively.

Solutions of the real part of Equation 6 are the dispersion relations for the upper-hybrid waves as well as for the Bernstein waves. Because in the present paper we are interested about these waves in the upper-hybrid band, where sometimes is a problem to distinguish between these waves, therefore in the following we use for them the common term: the electrostatic waves.

For the growth rate of these waves, we can write (Zheleznyakov & Zlotnik 1975a)

$$\gamma(\omega, k_{\perp}) = -\frac{\text{Im } \epsilon_{\parallel}^{(1)}}{\left[\frac{\partial \text{Re } \epsilon_{\parallel}^{(0)}}{\partial \omega} \right]_{\epsilon_{\parallel}^{(0)}=0}}. \quad (8)$$

In accordance with Kuznetsov (2005, Appendix A) the nominator of Equation 8 can be written as

$$\text{Im}(\epsilon_{\parallel}^{(1)}) = -2\pi^2 m_e^4 \frac{\omega_{pe}^2}{k^2} \sum_{l=s+1}^{\infty} ab^2 \int_0^{\pi} J_l \left(\frac{\gamma_{rel} k_{\perp} v_{\perp}}{\omega_{ce}} \right) \frac{\gamma_{rel}^5 \sin \phi}{\frac{\partial \psi}{\partial \rho}} \frac{l \omega_{ce}}{\gamma_{rel} v_{\perp}} \frac{\partial f}{\partial p_{\perp}} d\phi, \quad (9)$$

$$\frac{\partial \psi}{\partial \rho} = \frac{\gamma_{rel}^2 l \omega_{ce}}{c^2} (v_{\parallel}^2 + v_{\perp}^2), \quad (10)$$

$$v_{\parallel} = -a \cos(\phi), \quad v_{\perp} = b \sin(\phi), \quad (11)$$

$$a^2 = \frac{l^2 \omega_{ce}^2 c^2 (l^2 \omega_{ce}^2 - \omega^2)}{l^4 \omega_{ce}^4}, \quad (12)$$

$$b^2 = \frac{c^2 (l^2 \omega_{ce}^2 - \omega^2)}{l^2 \omega_{ce}^2}, \quad (13)$$

where c is the speed of light, v_{\parallel} and v_{\perp} are the velocities on resonance ellipse in Equation 2. f is the electron velocity distribution function in the form

$$f(v_{\perp}, v_{\parallel}) = f_0(v_{\perp}, v_{\parallel}) + \frac{n_h}{n_e} f_{hot}(v_{\perp}, v_{\parallel}). \quad (14)$$

The f_0 means the background Maxwellian distribution for temperature v_{tb} , f_{hot} is in our case the Dory-Guest-Harris distribution given by Equation 3 described by the "thermal" velocity v_t and $J_l(\lambda)$ is the Bessel function.

Furthermore, the denominator of Equation 8 can be expressed as

$$\frac{\partial \epsilon_{\parallel}}{\partial \omega} = 4\omega \omega_{pe}^2 \frac{e^{-\lambda}}{\lambda} \sum_{l=1}^{\infty} \frac{l^2 I_l(\lambda)}{(\omega^2 - l^2 \omega_{ce}^2)^2}. \quad (15)$$

Parameter	Value
v_{tb}	0.018 c (2 MK)
v_t	0.2 c
n_e/n_h	32
f_{hot}	DGH
ω_{pe}/ω_{ce}	4.0 – 5.3
$k_{\perp}c/\omega_{pe}$	0 – 15 range
ω/ω_{pe}	0 – 2 range

Table 1. Parameters used for computing of the growth rates.

3. ANALYTICAL GROWTH RATES

In this Section, we compute the growth rates using analytically derived equations expressed in the previous Section. As an example we make computations for the ratio of the electron-plasma and electron-cyclotron frequency (ω_{pe}/ω_{ce}) in the 4.0-5.3 range. Namely, we want to determine the growth rates also for a non-integer ratio of ω_{pe}/ω_{ce} . The relatively low values of this ratio are chosen due to a comparison with the numerical simulations, where computations with the low values of ω_{pe}/ω_{ce} are more reliable.

If we do not mention explicitly, in our analytical computations and also in the following numerical simulations, we use the parameters shown in Table 1. Considering the propagation of waves in the strictly perpendicular direction to the magnetic field ($k_{\parallel} = 0$) and using Equations 6 we compute their dispersion branches and growth rates in the $\omega - k_{\perp}$ domain.

Because we want the frequency precision of dispersion branches at least $10^{-8}\omega_{pe}$, we searched for a sufficient number l in relation 6. We increased l until the precision of a dispersion branch position was higher than $10^{-8}\omega_{pe}$. Thus, we got $l_{\max} = 40$ and in relation 6 we use the summation $\sum_{l=1}^{l_{\max}=40}$. The same number l is also used in the summation in Equation 9.

Roots of Equation 6 (dispersion branches) are searched numerically using the Levenberg–Marquardt damped root method (Levenberg 1944; Marquardt 1963; Moré et al. 1980; Press et al. 2007) from SciPy package in the Python. This method was selected for its good convergence properties and ability to find the most narrower branches. The minimization is made in variable ω . First, the $\omega - k_{\perp}$ domain is divided into the regular orthogonal grid, which gives starting values of ω and k_{\perp} for the algorithm. Typically, we use $10^3 - 10^4$ grid points in ω direction and 20 – 40 grid points in k_{\perp} . In each step the method computes gradients in the Jacobian matrix and by the gradient descent method it proceeds until the required precision of ω is obtained. In our case we set this precision as $10^{-8}\omega_{pe}$. From the last step in this procedure we get the covariance matrix, which represents the gradient in a neighborhood of the found solution. We take the inverted absolute value of this gradient as the "characteristic

width” of the dispersion branches, see the following. From physical point of view the ”characteristic width” of the dispersion branch is given by thermal fluctuations of the electron plasma density. This ”characteristic width” does not represent the actual relative frequency range occupied by the waves, but is rather proportional to that frequency range; the proportionality coefficient depends on many factors (fluctuations etc.), but its absolute value is unimportant for this study.

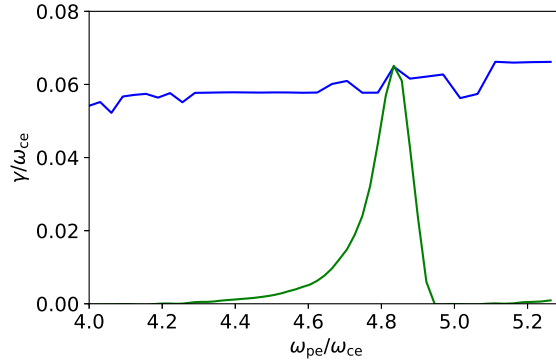


Figure 1. The maximal growth rate found at the upper-hybrid branch (Equation 1) (green line), and at all electrostatic branches (Equation 6) (blue line). The frequency and wave vector intervals are the same as for the integrated growth rate in Figure 2.

First, we compute the maxima of the growth rate γ at the upper-hybrid branch (Equation 1) in dependence on ω_{pe}/ω_{ce} . The result is shown in Figure 1 by the green line. Then using Equation 6 we compute the maximal growth rate at all electrostatic branches in the $\omega - k_{\perp}$ domain, see the blue line in Figure 1. Note that these maximal growth rates are always taken in one specific point of the $\omega - k_{\perp}$ domain. While the growth rate at the upper-hybrid branch has distinct maximum ($\gamma/\omega_{ce} \approx 0.06$) at about $\omega_{pe}/\omega_{ce} = 4.8$, the growth rates for all branches are similar. It means that at almost all branches in the $\omega - k_{\perp}$ domain there are positive growth rates.

Because our main goal is to compare the results obtained from analytical relations with those from the following PIC simulations, where the growth rate is given by compositions of growth rates in the whole $\omega - k_{\perp}$ domain, we define a new quantity – the integrated growth rate Γ as

$$\Gamma = \frac{1}{\Gamma_0} \int \gamma(\omega, k_{\perp}) \sigma(\omega, k_{\perp}) \delta(\epsilon_{\parallel}^{(0)}(\omega, k_{\perp})) d\omega dk_{\perp}, \quad (16)$$

where δ is the Dirac delta function and $\gamma(\omega, k_{\perp})$ is the growth rate at the specific ω and k_{\perp} . This integral counts the growth rates over the dispersion branches of the electrostatic waves in the whole $\omega - k_{\perp}$ domain with their ”characteristic width” σ . The function Γ_0 is the normalization factor

$$\Gamma_0 = \int \sigma(\omega, k_{\perp}) \delta(\epsilon_{\parallel}^{(0)}(\omega, k_{\perp})) d\omega dk_{\perp}. \quad (17)$$

In our case the integral is computed over the $\omega - k_{\perp}$ area with $\omega/\omega_{pe} \in (0, 2)$ and $k_{\perp}c/\omega_{pe} \in (0, 20)$. At higher frequencies the branches are very narrow and thus do not contribute effectively to the integrated growth rate and at higher values of the wave vectors $\gamma = 0$.

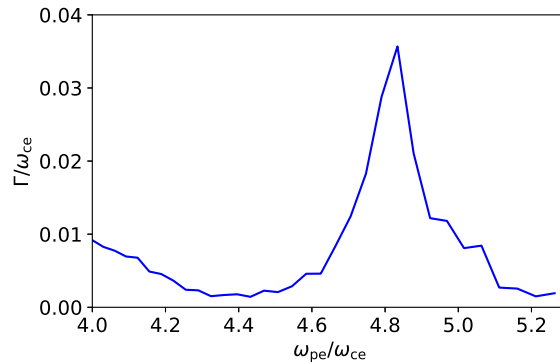


Figure 2. Integrated growth rate Γ computed from Equation 16 as a function of the ratio ω_{pe}/ω_{ce} normalized to ω_{ce} for the parameters given in Table 1. Its maximum is for $\omega_{pe}/\omega_{ce} = 4.8$ and minimum for $\omega_{pe}/\omega_{ce} = 4.4$.

Using the plasma parameters from Table 1 we computed the integrated growth rates Γ (Equation 16) for the ratios $\omega_{pe}/\omega_{ce} = 4.0 - 5.3$, see Figure 2. As can be seen in this figure, the maximum of Γ is for $\omega_{pe}/\omega_{ce} = 4.8$ and the minimum for $\omega_{pe}/\omega_{ce} = 4.4$.

Now, a question arises how the integrated growth rate Γ is related to the positions of dispersion branches in the $\omega - k_{\perp}$ domain. To answer this question, we compute the dispersion branches in the $\omega - k_{\perp}$ domain for the maximal and minimal values of the integrated growth rate Γ . We also plot growth rates in the whole domain $\omega - k_{\perp}$, although growth rates outside dispersion branches are non-physical. It is because the growth rates are defined only for roots of Equation 6. But, we use this type of presentation to show a relation between positions of dispersion branches and regions favorable for the wave amplification.

The results are shown in Figure 3, where the growth rates and dispersion branches are in a broad area of $\omega - k_{\perp}$ (Plots a, b). The detailed views are from the upper-hybrid band (Plots c, d). We note that the parts of dispersion branches with the "characteristic width" σ less than 10^{-6} are very narrow and thus they are not represented in the figure, see also the following and Table 2.

As seen here, in the $\omega - k_{\perp}$ domain there are the regions with the high growth rates. The maximal growth rate on dispersion curves in the field of view of Figure 3c is $\gamma/\omega_{ce} \approx 0.06$. Comparing the cases with the maximal and minimal integrated growth rates Γ , we can see differences in distributions of the dispersion branches and growth rate regions. While in the case with the maximal Γ the dispersion branches in most cases cross the region with the high growth rates γ , in the case with the minimal

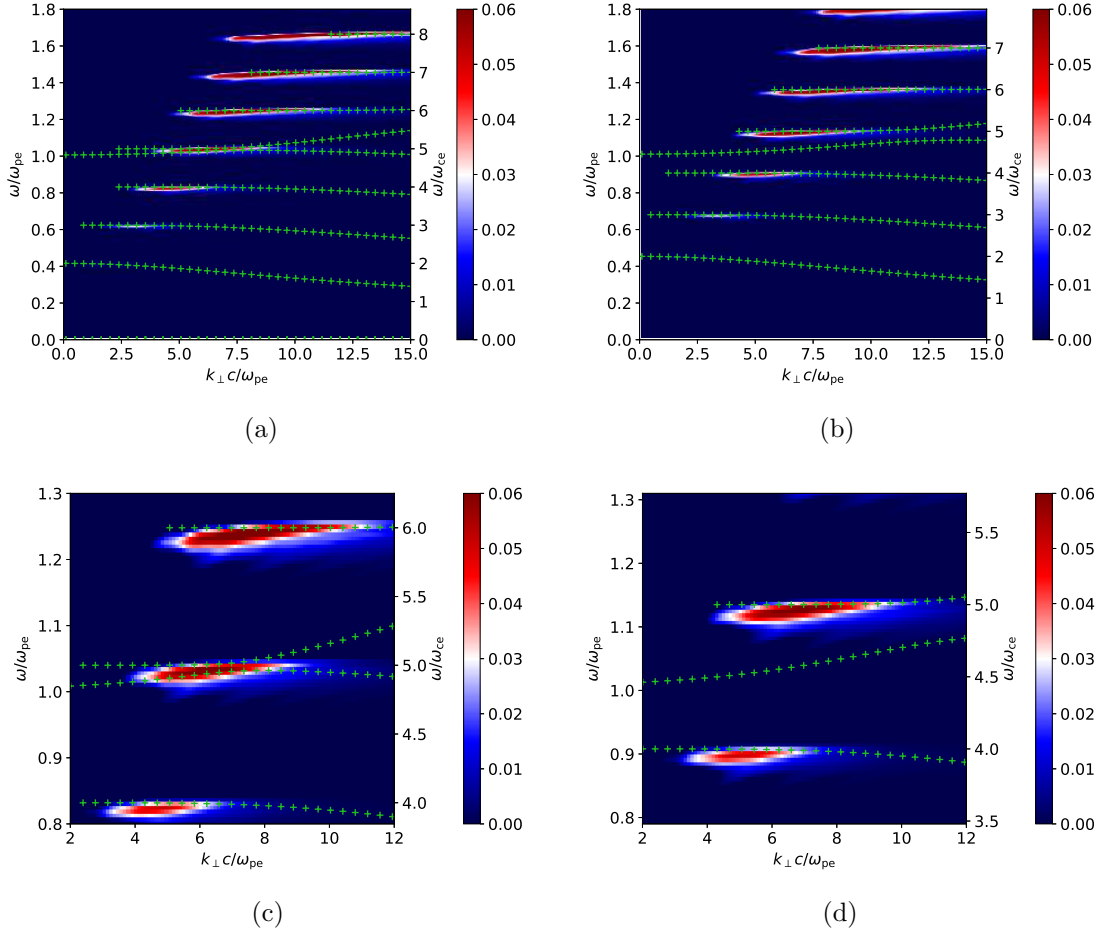


Figure 3. Analytical growth rates γ/ω_{ce} and dispersion branches in the $\omega - k_{\perp}$ domain (the blue-red scale) for the maximal value of Γ , i.e., for $\omega_{pe}/\omega_{ce} = 4.8$ (a, c) and for the minimal value of Γ , i.e., for $\omega_{pe}/\omega_{ce} = 4.4$ (b, d) taken from Figure 2. The green crosses show dispersion branches of the electrostatic waves. The growth rates and dispersion branches in a broad range of (ω, k_{\perp}) are in (a, b) and the same in a detailed view in the upper-hybrid band are in (c, d).

Γ the thickest branches are out these regions. Note that for the integrated growth rate it is important not only this crossing over these regions but also the lengths and width (area) of the dispersion branches over these regions. Namely, the wave energy is given by the wave energy density in the area unit times the area. We suppose that the width of the dispersion branch is proportional to σ calculated during computations of the dispersion branches. Thus, there are the dispersion branches, which go through the high growth rate regions even for the minimal growth rate Γ (see Figure 3b, e.g. the region $\omega/\omega_{pe} = 1.4$, $k = 6 - 15$), but their "characteristic width" is very small and therefore do not significantly influence the integrated growth rate Γ .

In the Table 2 we present the "characteristic width" of different dispersion branches σ . A difference in the "characteristic width" can be several orders. The maximal Γ appears, when the dispersion branch with the highest "characteristic width" crosses the high growth rate area around the plasma frequency, see Figure 3c. It is interesting

Maximum $\omega_{pe}/\omega_{ce} = 4.8$			Minimum $\omega_{pe}/\omega_{ce} = 4.4$		
$\omega_{branch}/\omega_{pe}$	$\omega_{branch}/\omega_{ce}$	σ	$\omega_{branch}/\omega_{pe}$	$\omega_{branch}/\omega_{ce}$	σ
0.334	1.603	7.4×10^{-3}	0.373	1.788	9.1×10^{-3}
0.593	2.846	1.0×10^{-2}	0.652	3.128	1.2×10^{-2}
0.821	3.943	1.2×10^{-2}	0.897	4.306	2.0×10^{-2}
1.030	4.945	9.9×10^{-2}	1.069	5.133	4.0×10^{-1}
1.076	5.164	3.4×10^{-1}	1.140	5.471	2.2×10^{-2}
1.250	6.001	6.6×10^{-4}	1.364	6.546	1.46×10^{-4}
1.456	6.989	1.5×10^{-5}	1.591	7.636	3.95×10^{-6}

Table 2. "Characteristic width" of the dispersion branches σ for the maximum Γ with $\omega_{pe}/\omega_{ce} = 4.8$ (see Figure 2) and for the minimal Γ with $\omega_{pe}/\omega_{ce} = 4.4$. ω_{branch} means the frequency of the dispersion branch for $k_{\perp}c/\omega_{pe} = 10$.

that in this case, two dispersion branches of the electrostatic waves are very close to each other.

To show how the dispersion branches change, in Figure 4 we present the dispersion branches for three values of the ratio $\omega_{pe}/\omega_{ce} = 4.925, 4.950$ and 4.975 . Here in the left part of the figure we can see that the dispersion branch, which is firstly under the plasma frequency, is going up to higher frequencies with decreasing ω_{pe}/ω_{ce} . During this shift it extrudes the upper dispersion branch up (Figure 4c). In the region where the branches meet a knee on the bottom dispersion branch is formed; i.e., for lower k_{\perp} than this knee there is a part of the dispersion branch with the normal dispersion and for higher k_{\perp} is the part with the anomalous dispersion (Figure 4c). Thus, in some cases, the electrostatic waves are generated at the part with the normal dispersion and in others at that with the anomalous dispersion.

For the value of $v_{tb} = 0.018 c$ considered in Figure 4a,c,e, this interplay of dispersion branches happens slightly out of the region with high growth rates; therefore the integrated growth rate Γ has not the maximal value. However, we found that for lower background thermal velocity ($v_{tb} = 0.007 c$), the dispersion branches not only meet, but they also are in the region with high growth rates (Figure 4d, f) and thus for these plasma parameters the high integrated growth rate Γ can be expected.

We also studied the distribution of the growth rates γ and dispersion branches in dependence on the background plasma temperature (Figure 5). With increasing the background plasma temperature the center of the region with the high growth rates remains at the same position, but the size of this region decreases. Moreover, the point, where dispersion branches meet and cross the region with the high growth rates, shifts to lower k_{\perp} . The reason is that for the constant $\lambda = k_{\perp}^2 v_{tb}^2 / \omega_{ce}^2$ the component of the wave vector k_{\perp} has to decrease when v_{tb} increases. It implies that for the dispersion branches close to the plasma frequency and $v_{tb} < 0.018 c$ the

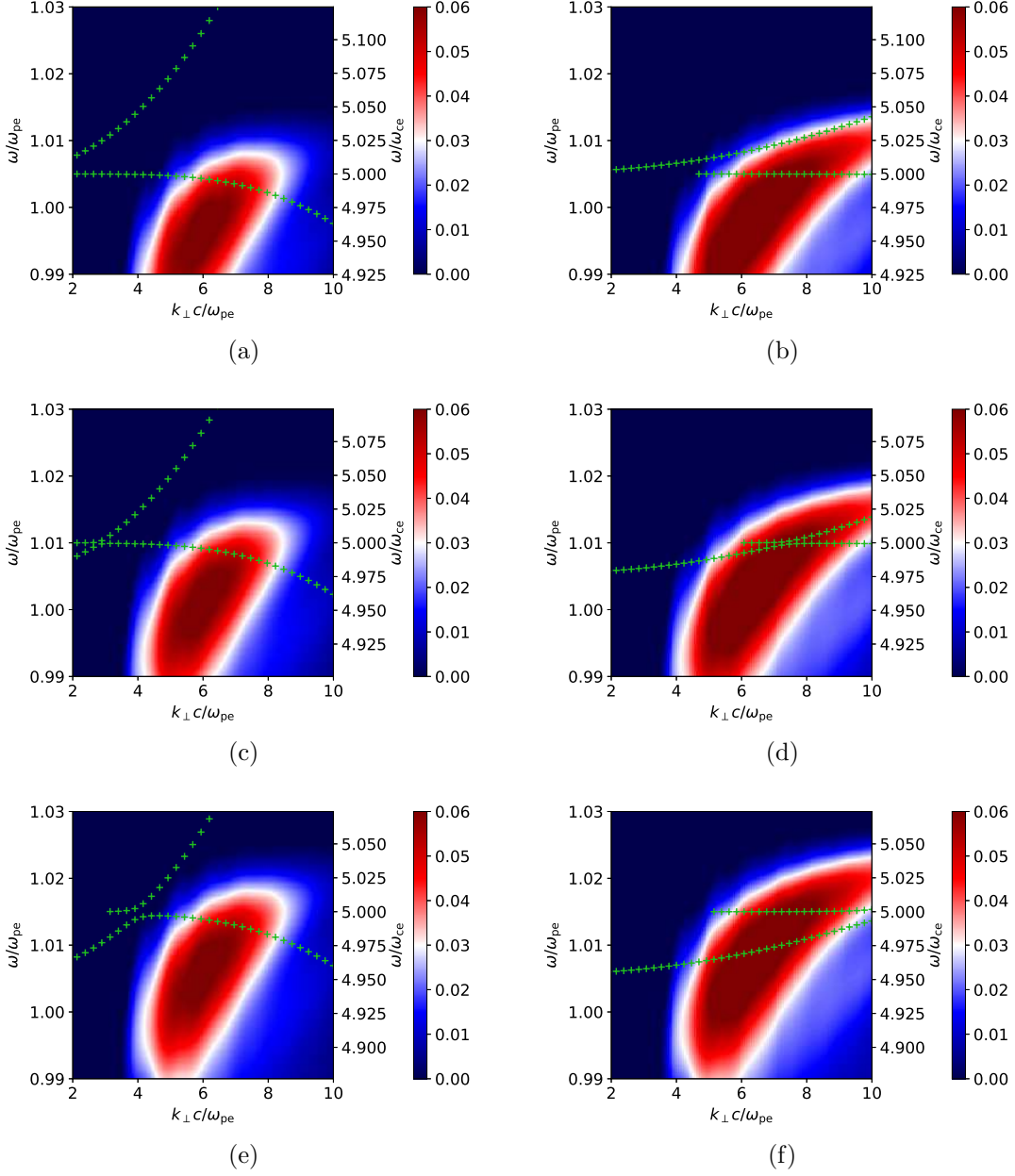


Figure 4. Analytical growth rates normalized to ω_{ce} and dispersion branches in dependence on ratio ω_{pe}/ω_{ce} and 4.975 (a, b), 4.950 (c, d), 4.925 (e, f) for two background temperatures: $v_{tb} = 0.018 c$ (a, c, e) and $v_{tb} = 0.007 c$ (b, d, f).

electrostatic waves are generated at the normal part of the dispersion branch, while for higher thermal velocities in its anomalous part.

On the other hand, Figure 6 shows the distribution of the growth rates and dispersion branches in dependence on the "thermal" velocity of hot electrons v_t . With increasing this velocity the position of the region with high growth rates shifts to lower k_{\perp} . For a constant argument in the Bessel function in Equation 9, $\text{const} = \Gamma v_{\perp} k_{\perp} / \omega_{ce}$, k_{\perp} decreases as v_{\perp} increases. The region with high growth rates expands along the frequency axis with increasing v_t . However, the maximal values of γ in the region

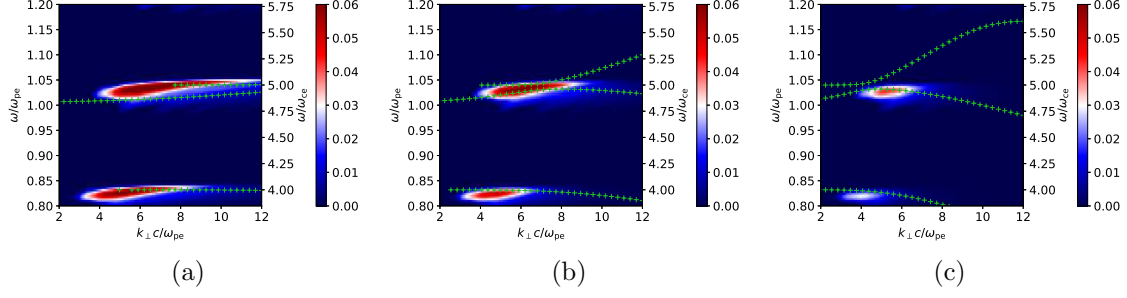


Figure 5. Analytical growth rates normalized to ω_{ce} (blue-red scale) and dispersion branches in dependence on the background thermal velocity: a) $v_{tb} = 0.007 c$, b) $v_{tb} = 0.018 c$, and c) $v_{tb} = 0.030 c$. The thermal velocity of the hot component $v_t = 0.2 c$ and $\omega_{pe}/\omega_{ce} = 4.8$ are kept constant in all these cases.

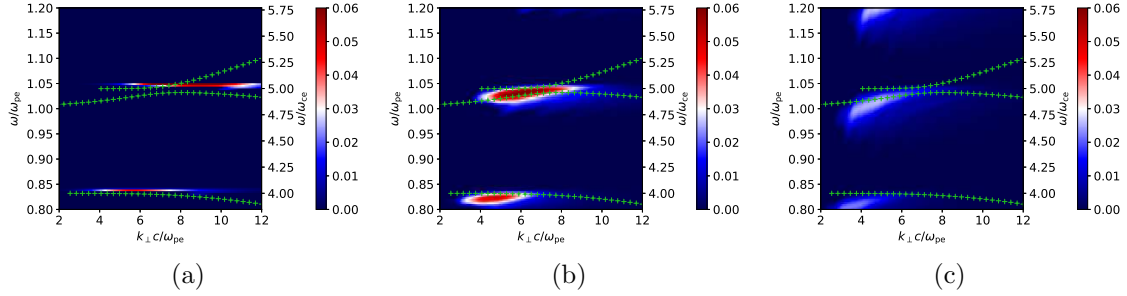


Figure 6. Analytical growth rates normalized to ω_{ce} and dispersion branches in dependence on the hot electrons velocity: a) $v_t = 0.1 c$, b) $v_t = 0.2 c$, and c) $v_t = 0.3 c$. $v_{tb} = 0.018 c$ and $\omega_{pe}/\omega_{ce} = 4.8$ are kept constant.

center decrease. The reason is that the value of the term $\partial f(v_{\perp}, v_{\parallel})/\partial v_{\perp}$ decreases with increasing of v_t . For temperatures $v_t < 0.15 c$ the area of the region with high growth rates γ is so narrow that the integrated growth rate Γ is without a distinct peak.

4. NUMERICAL GROWTH RATES IN THE PIC MODEL

We make simulations using a 3D Particle-in-Cell (PIC) relativistic model (Buneman & Storey 1985; Matsumoto & Omura 1993; Karlický & Bárta 2008; Benáček & Karlický 2018) with multi-core Message Passing Interface (MPI) parallelization. Further details can be found in Matsumoto & Omura (1993, p.67-84) and on the link below.¹

The model size is $48\Delta \times 48\Delta \times 16\Delta$ in x, y, z -directions respectively. The generated electrostatic waves are in $x - y$ plane, z coordinate corresponds to the magnetic field direction. One run takes 80 000 time steps with the time step $\omega_{pe}t = 0.025$. The electron distribution function is DGH distribution, the number of electrons per cell is

¹ <https://www.terrapub.co.jp/e-library/cspp/text/10.txt>.

$n_e = 960$, the ratio of densities of the background plasma and hot electrons is $n_e/n_h = 32$, $\omega_{pe}/\omega_{ce} = 4\text{-}5.3$. Other parameters are as in Table 1.

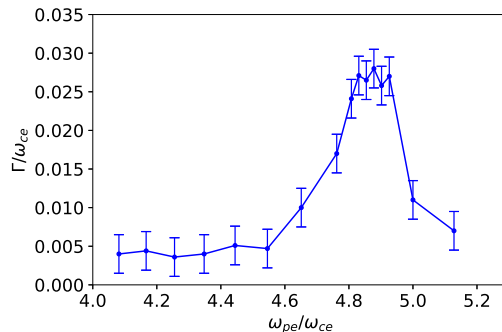


Figure 7. Growth rates from PIC simulations as a function of the ratio ω_{pe}/ω_{ce} for $v_t = 0.2 c$, $v_{tb} = 0.018 c$. Compare it with Γ in Figure 2.

Varying the ratio of ω_{pe}/ω_{ce} in the range 4.0-5.3 we made the PIC simulations and estimated the growth rates from the growth of the electrostatic wave energy (Figure 7). Note that these growth rates correspond to the integrated growth rates Γ in the analytical approach. The profile of the growth rate and the growth rate values are very similar to that presented in Figure 2. In the range of $\omega_{pe}/\omega_{ce} = 4.1 - 4.5$ the growth rate is very weak, and at $\omega_{pe}/\omega_{ce} = 4.88$ there is the growth rate maximum. It is at slightly higher values of ω_{pe}/ω_{ce} comparing with the maximum Γ shown in Figure 2.

5. DISCUSSION AND CONCLUSIONS

In this paper we computed two types of the growth rate: a) the growth rate γ that corresponds to one point in the $\omega - k_{\perp}$ domain, i.e., located at one specific dispersion branch and b) the growth rate Γ integrated over the upper-hybrid band, where we took into account the fact that in real conditions as well as in PIC simulations the instability can start simultaneously not only at one point in the $\omega - k_{\perp}$ domain, but in some area in this domain and even on several dispersion branches. While the maximal growth rate γ/ω_{ce} is found as about 0.06, the maximal integrated growth rate Γ/ω_{ce} is about 0.03. The maximal growth rate γ is similar to those presented by Zheleznyakov & Zlotnik (1975a); Winglee & Dulk (1986); Benáček et al. (2017), but due to various thermal velocities, plasma densities and magnetic fields used in these papers this comparison is not straightforward. For example, for the parameters as in our Table 1, Zheleznyakov & Zlotnik (1975a) and also Zlotnik & Sher (2009) found the maximal growth rate as $\gamma/\omega_{ce} \approx 0.03$, which is twice smaller than our maximal growth rate $\gamma/\omega_{ce} \approx 0.06$. The difference in these values is probably due to different computational precisions in these studies.

The integrated growth rate is the parameter allowing a direct comparison with the PIC simulations, contrary to the growth rates at one branch of the electrostatic waves (Zheleznyakov & Zlotnik 1975a; Winglee & Dulk 1986; Kuznetsov 2005;

Zlotnik & Sher 2009; Benáček et al. 2017), see also Aschwanden (1990). In computations of the integrated growth rate we use the "characteristic width" of dispersion branches. We think that this "characteristic width" is a result of thermal fluctuations of the electron plasma density. We found that the "characteristic width" can differ for different dispersion branches. Just these differences lead to the integrated growth rate Γ which agrees to that computed by PIC simulations. When we would use the constant "characteristic width" of dispersion branches ($\sigma = 1$) then the integrated growth rate would be without peaks at resonances.

We found that the profile of the integrated growth rate Γ obtained by analytical calculations and that in PIC simulations are very similar and their maxima are at almost the same value of ω_{pe}/ω_{ce} . This difference can be explained by slightly different positions of dispersion branches in the analytical and numerical approaches. Namely, the condition $n_h \ll n_e$ which is used in the analytical approach, in PIC simulations is difficult to fulfill, which has an impact on positions of dispersion branches in PIC model. We found that the growth rate peak in PIC simulations is broader than that in the analytical approach. We think that it is because in the PIC model there can also be the electrostatic waves with $k_{\parallel} \neq 0$.

We also compared the maximal Γ from the present PIC simulations with that in our previous paper (Benáček & Karlický 2018). We found that due to an error in the growth-rate normalization in our previous paper the growth rate in this paper was overestimated 20 times. Considering this correction the maximal growth rate Γ from the present paper agrees to that in the paper by Benáček & Karlický (2018).

In dispersion diagrams with dispersion branches, calculated analytically, we showed how the plasma parameters influence their positions in the $\omega - k_{\perp}$ domain. We found that when the dispersion branch with the sufficient "characteristic width" and length crosses the region with high growth rates then the integrated growth rate Γ is high.

Varying the plasma parameters, we showed that in some range of ω_{pe}/ω_{ce} the dispersion branches can meet and change the form to that with a knee. We found that sometimes a dominant contribution to the integrated growth rate Γ comes from the normal part of the dispersion branch and sometimes from the anomalous part. Moreover, when some branches meet then it is sometimes difficult to distinguish a type of the electrostatic wave.

We found that in the upper-hybrid band there can be several dispersion branches of the electrostatic waves perpendicular to the magnetic field with normal and anomalous dispersions. We showed that sometimes two branches can even meet in the $\omega - k_{\perp}$ domain. In the double plasma resonance (DPR) models of radio zebras only the instability of the upper-hybrid waves with the normal dispersion (Eq. 1) is considered. Thus, in new zebra models, instabilities on all branches in the upper-hybrid band should be taken into account. Although it complicates the models, especially analytical ones, they will be more realistic than the present models. New zebra models need to describe the processes in the whole upper-hybrid band, because for the

zebra emission the whole electrostatic wave energy, generated on different dispersion branches, is important. PIC models naturally solve this problem, but they also need to be improved.

We thank an anonymous referee for valuable comments. We acknowledge support from Grants 17-16447S, 18-09072S and 19-09489S of the Grant Agency of the Czech Republic. This work was supported by The Ministry of Education, Youth and Sports from the Large Infrastructures for Research, Experimental Development and Innovations project "IT4Innovations National Supercomputing Center – "LM2015070".

Software: Python, SciPy, Jupyter

REFERENCES

- Altyntsev, A. T., Kuznetsov, A. A., Meshalkina, N. S., Rudenko, G. V. & Yan, Y. 2005, A&A, 431, A1037
- Aschwanden, M. J. 1990, A&AS, 85, 1141
- Benáček, J. & Karlický, M. 2018, A&A, 611, A60
- Benáček, J., Karlický, M., & Yasnov, L. 2017, A&A, 555, A1
- Buneman, O. & Storey, L. R. O. 1985, Simulations of fusion plasmas by a 3-D, E-M particle code, Tech. rep.
- Chen, B., Bastian, T. S., Gary, D. E., & Jing, J. 2011, ApJ, 736, 64
- Chen, F. F. 1974, Introduction to plasma physics, Plenum Press, New York
- Chernov, G. 2011, Fine Structure of Solar Radio Bursts, Astrophysics and Space Science Library 375, Springer, Heidelberg
- Dory, R. A., Guest, G. E., & Harris, E. G. 1965, Physical Review Letters, 14, 131
- Fitzpatrick, R. 2015, Plasma physics: an introduction (CRC Press)
- Hankins, T. H. & Eilek, J. A. 2007, ApJ, 670, 693
- Hankins, T. H., Eilek, J. A., & Jones, G. 2016, ApJ, 833, 47
- Karlický, M. & Bárta, M. 2008, SoPh, 247, 335
- Karlický, M. & Yasnov, L. V. 2015, A&A, 581, A115
- Karlický, M. & Yasnov, L. V. 2018a, ApJ, 867, 28
- Karlický, M. & Yasnov, L. V. 2018b, A&A, 618, A60
- Kuznetsov, A. A. 2005, A&A, 438, 341
- Ledenev, V. G., Karlický, M., Yan, Y., & Fu, Q. 2001, SoPh, 202, 71
- Levenberg, K. A 1944, Quart. Appl. Math. 2, 164-168
- Marquardt, D. 1963, SIAM J. Appl. Math. 11, 431-441
- Matsumoto, H. & Omura, Y. 1993, Computer space plasma physics: simulation techniques and software, Terra Scientific Pub. Co, p.305
- Melrose, D. B. & Dulk, G. A. 1982, ApJ, 259, 844
- Moré, J. J. Garbow, B. S. & Hillstom, K. E. 1980, User guide for MINPACK-1, Argonne Nat. Lab., ANL-80-74, <http://cds.cern.ch/record/126569>
- Panchenko, M., Rošker, S., Rucker, H. O., et al. 2018, A&A, 610, A69
- Press, W. H. Teukolsky, S. A. Vetterling, W. T. & Flannery, B. P. 2007, Numerical Recipes 3rd Edition: The Art of Scientific Computing, Cambridge University Press, New York, NY, USA
- Winglee, R. M. & Dulk, G. A. 1986, ApJ, 307, 808
- Yasnov, L. V. and Benáček, J. and Karlický, M. 2017, SoPh, 292, 163
- Zaitsev, V. V. & Stepanov, A. V. 1983, SoPh, 88, 297

- Zheleznyakov, V. V. 1997, Radiation in astrophysical plasmas [in Russian]; Original Russian Title — “Izlucheniye v astrofizicheskoy plasme”
- Zheleznyakov, V. V. & Zlotnik, E. I. 1975a, SoPh, 43, 431
- Zheleznyakov, V. V. & Zlotnik, E. Y. 1975b, SoPh, 44, 461
- Zlotnik, E. Ya. & Sher, É. M. 2009, Radiophysics and Quantum Electronics, 52, 88
- Zlotnik, E. Y. 2013, SoPh, 284, 579
- Zlotnik, E. Y., Shaposhnikov, V. E., & Zaitsev, V. V. 2016, Journal of Geophysical Research (Space Physics), 121, 5307